Chemical Science

ROYAL SOCIETY OF CHEMISTRY

EDGE ARTICLE

View Article Online
View Journal | View Issue

Cite this: *Chem. Sci.*, 2025, **16**, 18411

All publication charges for this article have been paid for by the Royal Society of Chemistry

Stereoselective ring-opening polymerization of racemic ethylglycolide: precisely regulated polyester properties *via* stereomicrostructure control

Jinbo Hu,[ab] Xinyan Liu,[ab] Yeqi Du,[ab] Wenbo Wang,[ab] Tianchang Wang,[a] Hao Zhang,[a] Ranlong Duan, *[a] Xinchao Bian *[ab] and Xuesi Chen [ab]

Received 23rd July 2025
Accepted 2nd September 2025

DOI: 10.1039/d5sc05510e

rsc.li/chemical-science

The development of high-performance, renewable polyesters with tunable mechanical properties is critical for advancing sustainable materials to replace petroleum-based plastics. Herein, a conceptually simple but highly effective strategy was employed for the stereoselective ring-opening polymerization (ROP) of racemic ethylglycolide (*rac*-EtG), affording polyesters with diverse sequence structures and a record-high isotacticity (P_m up to 0.99) among ROP of glycolide-type monomers. Strikingly, a simple adjustment of the steric hindrance at the 3-position of the salicylaldehyde moiety enabled a tunable switch in the stereoselectivity exhibited by the catalyst from atactic to isotactic and further to heterotactic. By tuning the stereomicrostructure of the polymer, a remarkable transition in ductility from 2.8% to 2119% was achieved. Typically, isotactic-rich poly(ethylglycolide) (*ir*-PEtG) exhibited an elongation at break of 569.9 ± 36.5% while maintaining a tensile strength of 26.7 ± 0.9 MPa. Furthermore, we demonstrated that a balanced distribution of crystalline and amorphous domains in the polymer microstructure enables simultaneous tuning of both strength and toughness.

Introduction

With the depletion of petroleum resources and the worsening of environmental pollution, polyester materials derived from renewable resources attracted extensive research interest over the past several decades.[1–4] Among them, polylactic acid (PLA), a biomass-derived aliphatic polyester, has emerged as one of the most promising alternatives to petroleum-based plastics due to its excellent biocompatibility and biodegradability.[5,6] However, its poor toughness and limited mechanical properties pose critical challenges to its broader application.[7,8] An effective strategy for enhancing the performance of PLA is the precise modulation of its properties through rational molecular design.[9–11] Recent studies conducted by Baker,[12,13] Wu,[14–16] Wang[17,18] and our group have demonstrated that the properties of polymers synthesized *via* ring-opening polymerization (ROP) of substituted glycolide monomers can be finely tuned across a broad range. In particular, polymers bearing ethyl side groups exhibit mechanical performance comparable to that of commercial isotactic polypropylene (*it*-PP) and high-density polyethylene (HDPE).[19] Nonetheless, issues such as slow crystallization rates and low melting temperatures (T_m = 108 °C) remain significant barriers to practical applications.[20,21] Previous studies have shown that stereoselective polymerization of racemic monomers can afford isotactic multiblock polymers with significantly elevated melting points.[22] However, the relationship between the polymer sequence structure and its performance-especially mechanical behavior-remains inadequately understood. Therefore, the development of stereoselective polymerization methods for racemic ethylglycolide (*rac*-EtG) to obtain stereoregular polyesters and elucidate the impact of the polymer microstructure on material properties holds considerable scientific importance and application potential.

The key to synthesizing polymers with distinct sequence structures *via* stereoselective polymerization of racemic monomers lies in the rational design of the catalyst architecture. Over the past thirty years, the scope of catalysts and racemic monomers utilized in stereoselective ROP has been extensively explored.[23,24] Organometallic catalysts, owing to their intrinsic high efficiency and selectivity, were widely favored by researchers.[25,26] Structurally, these catalysts could be classified as either chiral or achiral, and the stereoselectivity of the polymerization process was generally governed by one of two primary mechanisms: the chain-end control (CEC) mechanism or the enantiomorphic site control (ESC) mechanism.[27] In 1996, Spassky *et al.*[28] first reported the stereoselective ROP of *rac*-

[a]*State Key Laboratory of Polymer Science and Technology, Changchun Institute of Applied Chemistry, Chinese Academy of Sciences, 5625 Renmin Street, Changchun 130022, China. E-mail: xcbian@ciac.ac.cn*

[b]*School of Applied Chemistry and Engineering, University of Science and Technology of China, Hefei 230026, P. R. China*

lactide (*rac*-LA) using a chiral binaphthyldiamine-based salen–Al complex, which yielded PLA stereocomplexes with T_m as high as 187 °C. Subsequently, Coates,[29–32] Feijen,[33,34] Chen,[35–39] Kol,[40–42] and many other excellent scientists[43–46] developed a series of chiral catalysts for the stereoselective ROP of *rac*-LA, racemic propylene oxide (*rac*-PO), and racemic cyclic diolide (*rac*-DL). More recently, Wang and co-workers achieved a significant breakthrough in the stereoselective ROP of glycolide-type monomers by employing an innovative dual-ligand strategy, which enabled the kinetically perfect resolution polymerization of racemic phenethylglycolide.[17] It is worth noting, however, that such chiral catalysts, which functioned through the ESC mechanism, typically resulted in a maximum conversion of approximately 50%, leaving a substantial amount of unreacted monomer that required additional processing, thus increasing both production cost and process complexity.

To overcome this limitation, considerable efforts were devoted to investigating the catalytic performance of achiral catalysts in stereoselective ROP.[47,48] These catalysts are capable of simultaneously polymerizing both enantiomers of the monomer and typically operate by a CEC mechanism, leading to the formation of polymers with diverse stereochemical microstructures. However, the correlation between catalyst architecture, polymer sequence structure, and resulting material properties remains poorly understood (Scheme 1A). Furthermore, although highly isotactic polymers often exhibit elevated melting points due to their regular backbone packing,[49] effective catalyst systems capable of inducing high isotacticity in the ROP of glycolide-type monomers remain rare.

In this work, structurally simple mononuclear salen–Al complexes were employed to catalyze the stereoselective ROP of *rac*-EtG, affording polyesters with varied and well-defined chain microstructures. In addition to systematically investigating the influence of the catalyst backbone and substituents on the stereoselectivity of *rac*-EtG polymerization, another motivation for this study is to improve the thermal properties of PEtG by synthesizing highly isotactic PEtG (*it*-PEtG). Finally, by synthesizing PEtG samples with distinct sequence structures, we provide an in-depth discussion of the relationship between the stereochemical microstructure of the polymers and their resulting physical properties (Scheme 1B).

Results and discussion

Stereoselective ROP of *rac*-EtG

To achieve a highly isotactic selectivity system for the ROP of *rac*-EtG, we synthesized 17 salen–Al complexes, in which the length and nature of the phenoxy substituents and the diimino-linking units are varied (Scheme 2 and Fig. S1–S34). Subsequently, the ROP of *rac*-EtG was analyzed at 60 °C under conditions where the ratio of $[rac\text{-EtG}]_0/[\text{salen–Al}]_0/[\text{BnOH}]_0$ was 50/1/1. The corresponding stereoselectivity ROP of *rac*-EtG was investigated as shown in Table 1. Considering the prominent stereoselectivity of chiral catalysts in the ROP of cyclic lactone monomers, we initially evaluated the catalytic performance of classical chiral catalysts. At the outset, chiral cyclohexanediamine-based complexes were employed for the stereoselective ROP of *rac*-EtG (Table 1, entries 1 and 2). The **1a**/BnOH system exhibited low reactivity in the ROP of *rac*-EtG in toluene at 60 °C, achieving only 13.4% conversion after 192 h. When the substituent on the complex was changed to Br, a significant enhancement in catalytic activity was observed, with over 90% conversion attained within 68 h, affording PEtG with a high melting point and a slightly broad dispersity (T_m = 166 °C and $Đ$ = 1.28). The stereoregularity of the resulting PEtG was analyzed by quantitative ^{13}C NMR spectroscopy (Fig. 1A), and the P_m was calculated based on the ESC statistics (Fig. 1B and Table S1).[50] The pronounced [mmm] tetrad peak indicated

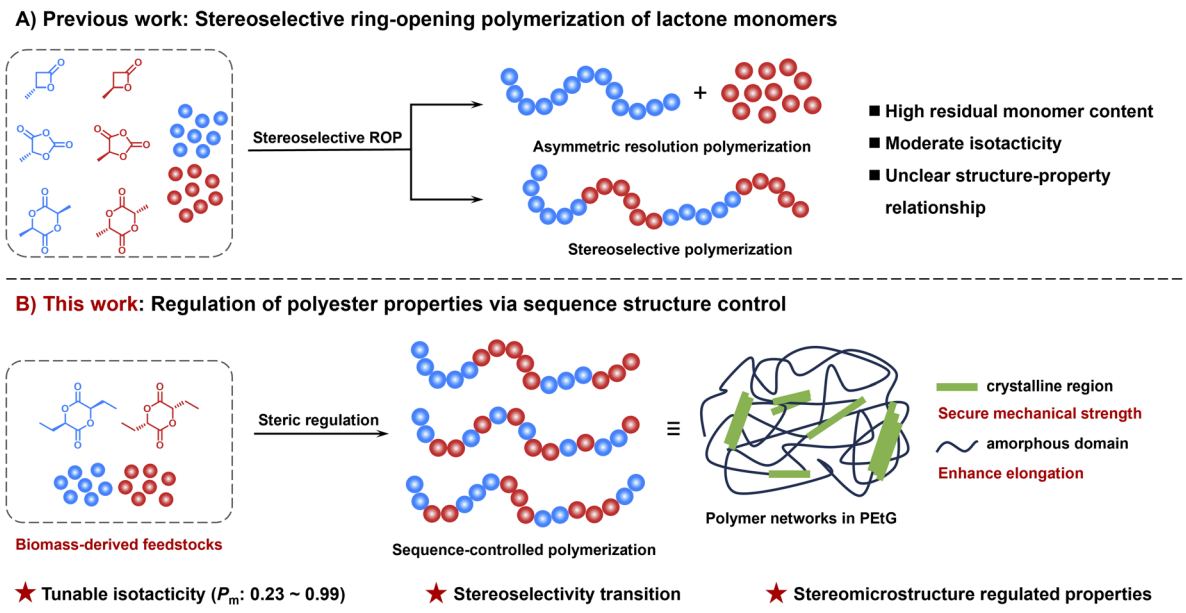

Scheme 1 Stereoselective ring-opening polymerization of lactones for sequence-controlled polyester synthesis.

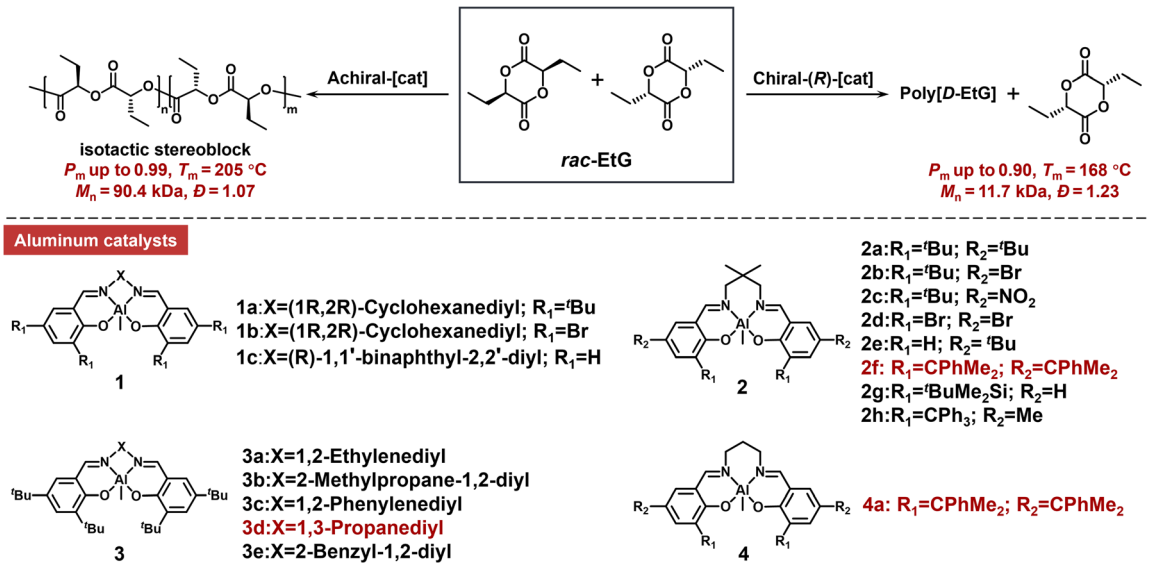

Scheme 2 Salen–Al mediated stereoselective ROP of *rac*-EtG.

an isotactic-rich architecture (*ir*-PEtG) derived from **1b**, with a P_m value of 0.88 (Fig. S35). We further explored chiral binaphthyl-based catalysts, which have been reported as effective for the ROP of cyclic lactones.[51] The result showed that **1c** exhibited lower catalytic activity than **1b**, but yielded PEtG with slightly higher isotacticity (Table 1, entry 3 and Fig. S36), suggesting that a relatively slower polymerization rate may be beneficial for improving polymer stereoregularity.

To further investigate the mechanism that chiral catalysts may follow in the ROP of *rac*-EtG, kinetic studies were conducted using **1b** and **1c** to catalyze the polymerization of different enantiomers of EtG. As shown in Fig. 1C and D, the chiral catalysts exhibited significantly different polymerization rates for the different enantiomers. The first-order kinetic results of the polymerization process indicated that (*R*)-salen–Al consistently showed a pronounced preference for *D*-EtG, resulting in faster polymerization rates, while *L*-EtG underwent slower polymerization, particularly with the chiral binaphthyl-based catalyst **1c**. The selectivity factor *s* ($s = k_L/k_D$) for **1c** was as high as 17.9. Moreover, the ROP of *rac*-EtG revealed a first-

Table 1 Aluminum-catalyzed ring-opening polymerization of *rac*-EtG[a]

Entry	Catalyst	$[M]_0/[Cat.]_0/[I]_0$	Temp. (°C)	*t* (h)	Conv.[b] (%)	$M_{n,theo.}$[c] (kDa)	$M_{n,GPC}$[d] (kDa)	Đ[d]	T_m[e] (°C)	P_m[f]
1	**1a**	50 : 1 : 1	60	192	13.4	1.1	—	—	—	—
2	**1b**	50 : 1 : 1	60	68	92.5	8.0	12.0	1.28	162	0.88
3	**1c**	50 : 1 : 1	70	125	93.1	8.0	11.7	1.23	168	0.90
4	**2a**	50 : 1 : 1	60	33	91.7	7.9	11.5	1.07	191	0.94
5[g]	**2a**	500 : 1 : 1	60	128	88.9	76.4	88.7	1.10	183	0.92
6	**2b**	50 : 1 : 1	60	33	91.8	7.9	11.7	1.06	184	0.92
7	**2c**	50 : 1 : 1	60	33	92.3	7.9	11.5	1.12	178	0.91
8	**2d**	50 : 1 : 1	60	1	96.3	8.3	12.2	1.08	111	0.79
9	**2e**	50 : 1 : 1	60	4.5	93.3	8.0	11.6	1.09	—	0.66
10	**2f**	50 : 1 : 1	60	45	93.1	8.0	11.8	1.08	194	0.96
11	**2g**	50 : 1 : 1	60	120	91.6	7.9	11.5	1.07	92	0.73
12	**2h**	50 : 1 : 1	60	168	83.9	7.2	9.5	1.12	—	0.27[h]
13	**2h**	50 : 1 : 1	80	96	91.8	7.9	11.5	1.07	—	0.30[h]
14	**2h**	50 : 1 : 1	50	288	86.2	7.4	10.1	1.10	—	0.23[h]
15	**3d**	50 : 1 : 1	60	33	90.2	7.8	11.1	1.10	192	0.95
16	**3e**	50 : 1 : 1	60	72	87.2	7.5	10.0	1.08	165	0.89
17	**4a**	50 : 1 : 1	60	45	92.3	7.9	11.6	1.07	194	0.96
18	**4a**	50 : 1 : 1	40	144	91.1	7.8	11.0	1.08	205	0.99
19[g]	**4a**	500 : 1 : 1	60	192	90.5	77.8	90.4	1.08	189	0.94
20[g]	**2d**	500 : 1 : 1	60	12	96.5	83.0	100.2	1.12	—	0.76

[a] Polymerization conditions: $[M]_0 = 1.0$ M, solvent = Tol. [b] Determined by ^{1}H NMR analysis of the reaction mixture. [c] $M_{n,theo.} = ([M]_0/[I]_0) \times$ Conv.% $\times M_w$ (EtG) + M_w (BnOH). [d] Measured by SEC (THF, 40 °C) and PS calibration. [e] T_m determined by DSC. [f] P_m represents the probability of mid-chain linkages between monomeric units, as determined by ^{13}C NMR analysis in the methylene region of PEtG, based on the ESC statistics. [g] $[M]_0 = 2.0$ M. [h] Calculations based on the CEC statistics.

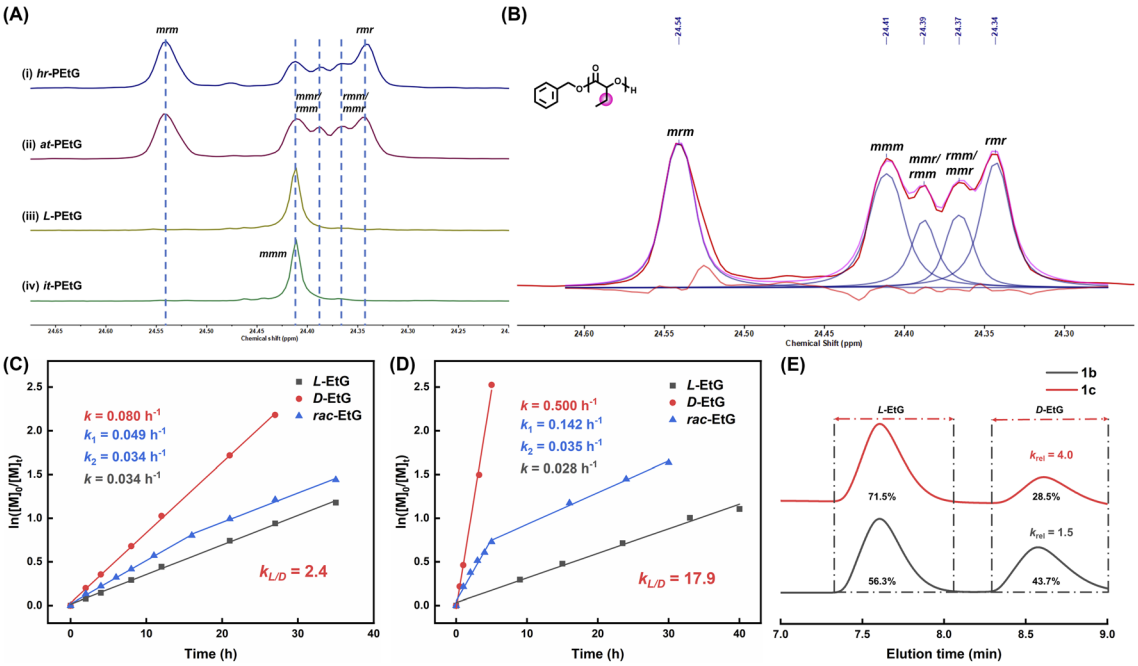

Fig. 1 (A) Quantitative ^{13}C NMR spectrum of PEtG in the methylene region: (i) *hr*-PEtG obtained using **2h** (Table 1, entry 12), (ii) *at*-PEtG obtained using $Sn(Oct)_2$ (Table **S2**, entry 22), (iii) *L*-PEtG obtained using $Sn(Oct)_2$ (Table S2, entry 23) and (iv) *it*-PEtG obtained using **4a** at 40 °C (Table 1, entry 18). (B) Methylene region of the quantitative ^{13}C NMR spectrum of atactic PEtG obtained by $Sn(Oct)_2$ catalyzed ROP of *rac*-EtG. (C) Kinetic study of EtG polymerization mediated by **1b** and (D) **1c**. Conditions: $[EtG]_0/[Cat.]_0/[BnOH]_0 = 50/1/1$, 60 °C, $[EtG]_0 = 1.0$ M in toluene. (e) ee values of the unreacted monomer. Black line: 49.1% conversion and ee = 12.6%; red line: 48.7% conversion and ee = 43.0%.

order kinetic profile with two approximately linear phases, where a reduction in the polymerization rate was observed after approximately 50% monomer conversion. This deceleration was attributed to the preferential consumption of a given enantiomer by the chiral salen–Al catalyst, which also aligned with the polymerization kinetics observed for pure enantiomers. These experimental results suggested that the chiral salen–Al catalysts may follow the ESC mechanism during the ROP of *rac*-EtG.

According to a strict ESC mechanism, one enantiomer was preferentially consumed, while the other remained largely unreacted until the favored enantiomer was nearly exhausted, ultimately yielding a polymer with high stereoregularity. To further validate this mechanism, we used chiral HPLC to determine the enantiomeric excess (ee) of the remaining monomer at 50% monomer conversion, and the enantiomeric selectivity of the catalysts was evaluated *via* the kinetic resolution coefficient (k_{rel}), which was calculated using Kagan's equation: $k_{rel} = \ln[(1-c)/(1-ee)]/\ln[(1-c)/(1+ee)]$,[52] where c is the monomer conversion. As shown in Fig. 1E, the k_{rel} values for complexes **1b** and **1c** were 1.5 and 4.0, respectively. The relatively low k_{rel} values suggested that the synthesis of highly isotactic polyesters *via* the structurally simple mononuclear chiral salen–Al catalysts was quite challenging. It was worth noting that the k_{rel} values obtained from the ee calculations differed from the s determined through kinetic experiments, which indicated that these chiral catalysts in the ROP of *rac*-EtG were co-controlled by both ESC and CEC mechanisms.[18,40] This conclusion was also consistent with the relatively low melting points observed for the resulting polymers.

Since it was challenging to obtain highly *it*-PEtG when the polymerization mediated by chiral catalysts was simultaneously governed by both ESC and CEC mechanisms, we shifted our focus to achiral mononuclear salen–Al catalysts, which are more likely to operate under CEC control in the polymerization of racemic monomers. It is worth noting that these catalysts can be synthesized in high yields (61–85%, see the SI for details) through a straightforward, established procedure using commercially available diamine compounds and salicylaldehyde derivatives.

Initially, the activity and stereoselectivity of the complex **2a** were investigated for the ROP of *rac*-EtG. Excitingly, high conversion of 50 equivalents of *rac*-EtG was achieved within a short time. As the [*rac*-EtG]/[**2a**] ratio was increased from 50/1 to 500/1, the molecular weight of the resulting PEtG increased from M_n = 11.5 kDa ($Đ$ = 1.07) to M_n = 88.7 kDa ($Đ$ = 1.10). More importantly, according to DSC and ^{13}C NMR analyses, when the [*rac*-EtG]/[**2a**] ratio was 50/1, **2a** produced *it*-PEtG with a T_m of up to 191 °C and a P_m of 0.94. Even for high molecular weight PEtG, a high stereoregularity (P_m = 0.92) was maintained (Table 1, entries 4–5 and Fig. S37). This was likely because the achiral salen–Al complexes predominantly followed the CEC mechanism for the stereoselectivity of the *rac*-EtG polymerization (Fig. S51). The larger steric hindrance of *rac*-EtG, combined with the bulky substituents of **2a**, synergistically enhanced the catalyst selectivity for the same type of chiral monomer, thereby leading to the formation of PEtG with high isotacticity.

To verify this hypothesis, we thoroughly investigated the effects of the electronic effects, steric effects, and the geometry of the skeleton diamine linkers in the salen ligand framework on the polymerization activity and stereoselectivity of *rac*-EtG. Regarding the electronic effects, electron-withdrawing substituents (Br and NO_2) at the 5-position of the salicylaldehyde moiety slightly decreased the stereoregularity of the resulting polymers (Table 1, entries 6–7), while the polymerization rates of **2b** and **2c** were slightly higher than that of **2a** (Fig. 2A). Notably, complex **2d**, bearing 3,5-dibromo substituents, exhibited a dramatically increased polymerization rate, reaching over 96% conversion within just 1 h. Kinetic studies showed that the polymerization rate of **2d** was approximately 44 times faster than that of **2a**. However, unfortunately, the polymer chain regularity obtained from **2d** was relatively poor (P_m = 0.79, Table 1, entry 8). These results clearly highlight the important influence of electron-withdrawing groups on polymerization activity in *rac*-EtG stereoselective ROP.

After establishing the influence of electronic effects on the ROP process, we shifted our focus to the steric effects of the catalyst. By simply replacing the *ortho*-substituent of the phenoxy group with a hydrogen atom, complex **2e** exhibited a significant increase in polymerization activity compared to **2a**, but with a notable decrease in selectivity (Table 1, entry 9). The resulting sequence structure exhibited characteristics typical of a random polymer (Fig. S41). Notably, although the higher polymerization activity of **2d** is generally unfavourable for isotactic selectivity, its larger steric hindrance from the *ortho*-positioned Br atoms leads to a higher isotactic selectivity compared to **2e** (Fig. S52), suggesting that the steric hindrance of the *ortho*-substituent on the phenoxy group is crucial for isotactic selectivity. To further enhance the stereoregularity of the resulting polymers, we attempted to increase the steric bulk of the *ortho*-substituents on the phenoxy group. Initially, we synthesized catalyst **2f** bearing a bulky $CPhMe_2$ group and investigated its catalytic performance. Notably, **2f** exhibited excellent isotactic selectivity, affording *it*-PEtG with a P_m up to 0.96 under conditions at 60 °C (Table 1, entry 10). When the steric hindrance was further increased to obtain catalyst **2g**, a decrease in polymerization activity was observed compared to **2f**. Contrary to our expectations, the isotactic selectivity of **2g** did not improve but instead declined significantly (Table 1, entry 11), despite this catalyst having previously demonstrated excellent isotactic control in the stereoselective ROP of *rac*-LA.[47] These results suggested that, in the stereoselective ROP of *rac*-EtG, the isotacticity of the resulting polymer does not increase

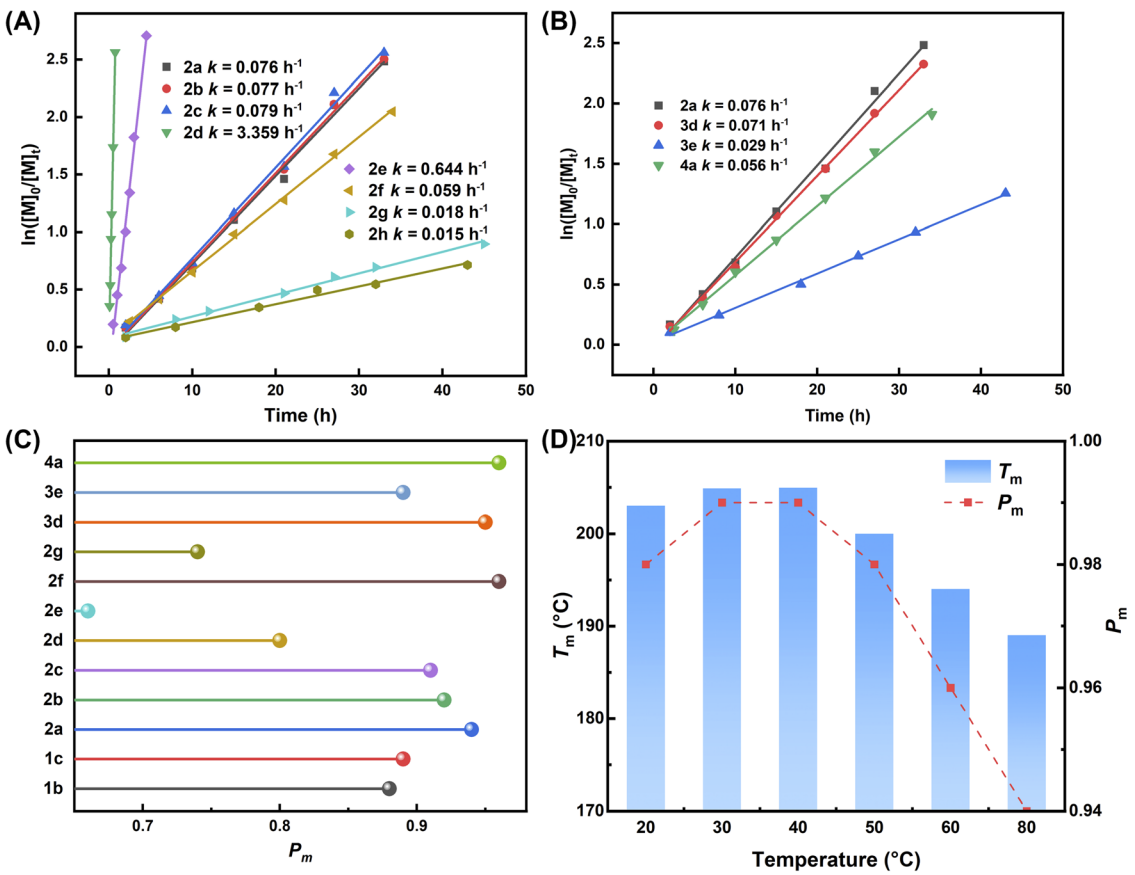

Fig. 2 (A) Kinetic study of *rac*-EtG polymerization mediated by salen–Al catalysts with different substituents. (B) Kinetic study of *rac*-EtG polymerization mediated by salen–Al catalysts with different main chain backbone linkages. Conditions: $[rac\text{-EtG}]_0/[\text{Cat.}]_0/[\text{BnOH}]_0 = 50/1/1$, 60 °C, $[rac\text{-EtG}]_0 = 1.0$ M in toluene. (C) Isotactic selectivity of various salen–Al catalysts. (D) **4a**-mediated plots of polymer T_m and P_m *versus* polymerization temperature. From left to right, the samples correspond to Table S2, entry 7; Table S2, entry 8; Table 1, entry 18; Table S2, entry 9; Table 1, entry 17 and Table S2, entry 10.

monotonically with the steric bulk of the catalyst *ortho*-substituents.

To further elucidate the relationship between *ortho*-position steric hindrance and the isotacticity of the resulting polymer, an additional steric bulk was introduced by synthesizing a salen–Al complex **2h**, bearing a bulky triphenylmethyl (Ph_3C) substituent at the 3-position. Polymerization kinetics revealed that the polymerization rate of **2h** was significantly lower than that of **2a** ($k_{2h} = 0.015\ h^{-1}$ and $k_{2a} = 0.076\ h^{-1}$). Interestingly, the polymer produced using complex **2h** at 60 °C exhibited a markedly different stereochemical structure. Quantitative ^{13}C NMR spectroscopy showed a significant increase in the tetrad signals corresponding to [mrm] and [rmr] (Fig. S44). The calculated probability of racemic linkages (P_r) equal to 0.73 based on the CEC statistics indicated that **2h**, with its bulky Ph_3C substituent, exhibited a certain degree of hetero-enrichment stereoselectivity (Table 1, entry 12). On one hand, the large *ortho*-substituent near the chain end created excessive steric congestion around the active site, which likely interfered with pre-coordination between the monomer and the metal center during polymerization.[53] On the other hand, the notably slow polymerization rate of **2h** may have hindered the continuous insertion of monomers with the same chirality, as this would increase the relative concentration of monomers with opposite configurations in the remaining monomers. As a result, insertion of monomers with opposite chirality at the chain end became more favorable, leading to a shift in selectivity and the formation of heterotactic-rich PEtG (*hr*-PEtG) (Fig. 3A). When the polymerization rate of **2h** was increased, its heterotactic selectivity decreases, whereas lowering the rate enhanced heterotacticity-further supporting our hypothesis (Table 1, entries 13–14). Additionally, similar switchable polymerization behavior induced by steric hindrance was recently reported by Wang,[18] Rieger, and co-workers.[54] In summary, these findings demonstrated that the size of the *ortho*-substituent on the phenoxy group had a significant impact on stereoselectivity. To further quantify the steric effect, we performed buried volume (% V_{Bur}) analysis using the SambVca 2.1 program ($r = 4.5$ Å),[55,56] which provides a reliable measure of ligand steric hindrance (Fig. 3B). The results revealed that **2h** exhibited a much larger buried volume (% V_{Bur} = 71.3%) compared with the other catalysts, confirming its higher steric hindrance that caused the observed selectivity inversion. Substituents of moderate steric bulk were found to be particularly favorable for enhancing the isotactic selectivity of salen–Al complexes. More importantly, a systematic variation in steric hindrance enabled a tunable

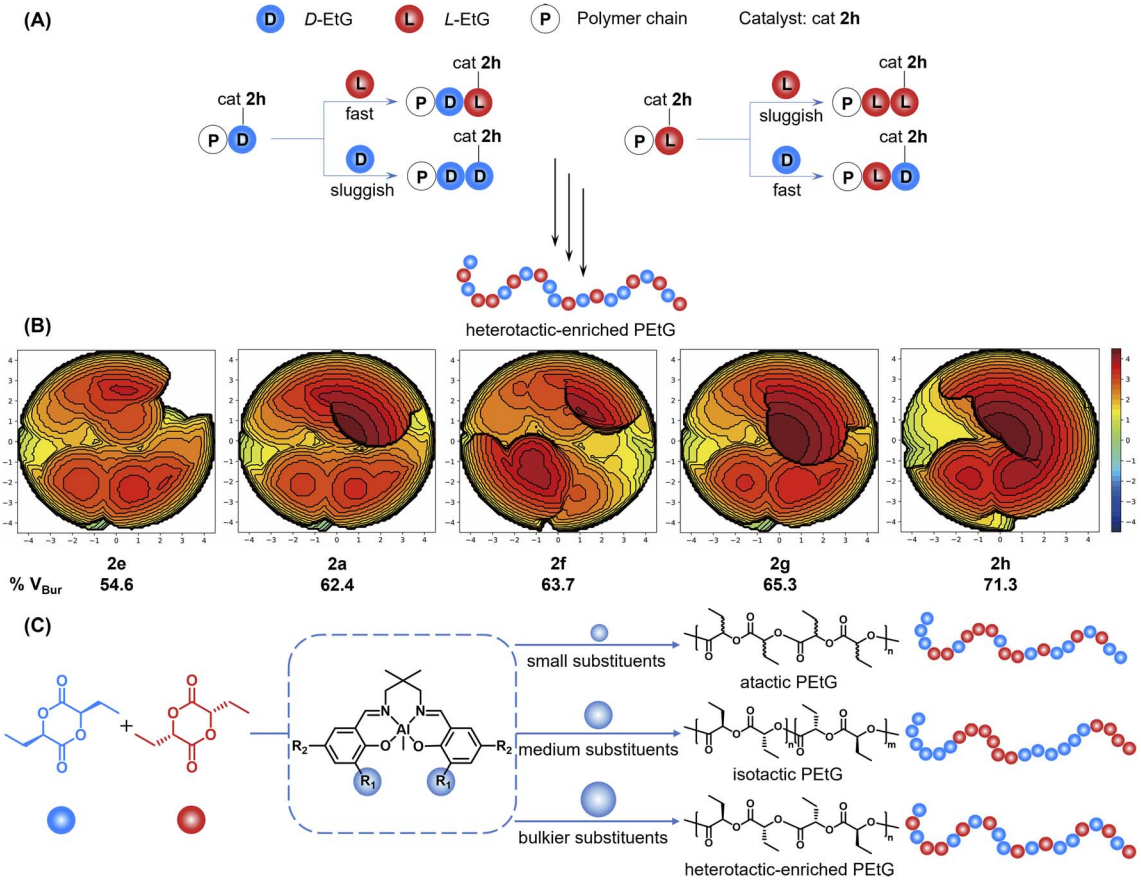

Fig. 3 (A) Schematic diagram of the possible mechanism of *rac*-EtG ROP catalyzed by cat **2h** to form heterotactic-enriched polymers. (B) Buried-volume analysis. The percentage of buried volume (% V_{Bur}) was calculated using the SambVca 2.1 web-based program with a sphere radius of 4.5 angstroms. (C) Stereoselective ROP of *rac*-EtG using salen–Al complexes yielding different sequences depending on the phenoxy *ortho*-substituent.

transition in the polymer microstructure from atactic to isotactic to heterotactic sequences (Fig. 3C).

With the optimal substituent on the salicylaldehyde framework determined, we finally explored the possible impact of the backbone linker on the polymerization process. Shortening the backbone to C_2 linkers, such as 1,2-ethylenediyl (**3a**) and 2-methylpropane-1,2-diyl (**3b**), caused a significant reduction in the polymerization activity, with less than 10% monomer conversion achieved after over 120 h of polymerization (Table S2, entries 1–2). For the sample catalyzed by the phenyl-based backbone catalyst (**3c**), a similar polymerization rate to **3a** and **3b** was observed (Table S2, entry 3). When the backbone was extended to a C_3 linker, 1,3-propanediyl (**3d**) yielded *it*-PEtG with a P_m of 0.95 at 60 °C (Table 1, entry 15). On keeping the C_3 backbone but introducing a phenyl substituent, catalyst **3e** exhibited a decrease in polymerization activity (Fig. 2B), and the isotacticity of the resulting polymer also significantly decreased (Table 1, entry 16). Overall, the polymer chain regularity generally increased with the flexibility of the backbone linker (Fig. 2C),[48] which was likely attributed to the enhanced conformational adaptability of the metal complex, facilitating the geometric requirements of key transition states involved in the ROP process.

Based on the combined evaluation of salicylaldehyde substituents and amine-bridged backbones in the stereoselective ROP of *rac*-EtG, complex **4a** was ultimately synthesized and its catalytic behavior was investigated. As anticipated, under the same conditions, **4a** exhibited the highest isotactic selectivity, affording highly *it*-PEtG with a P_m of up to 0.96 within a relatively short reaction time, while maintaining a narrow molecular weight distribution (Table 1, entry 17, Fig. S46). The catalyst also demonstrated excellent control over molecular weight. By varying the feed ratio of $[rac\text{-EtG}]_0/[\mathbf{4a}]_0/[I]_0$ from 50/1/1 to 500/1/1, the M_n of the resulting polymers increased linearly from $M_n = 11.1$ kDa ($Đ = 1.10$) to $M_n = 90.4$ kDa ($Đ = 1.08$) (Fig. S53B), and GPC traces showed unimodal distributions. Remarkably, all PEtG samples obtained under these conditions exhibited high stereoregularity ($P_m = 0.94$–0.95) and elevated melting points ($T_m = 189$–193 °C), indicating that **4a** maintained excellent stereocontrol throughout the polymerization. The controlled nature of the **4a**-mediated ROP was further confirmed by matrix-assisted laser desorption/ionization time-of-flight mass spectrometry (MALDI-TOF-MS) (Fig. S53C). Together, these results demonstrate that the ROP of *rac*-EtG mediated by **4a** exhibits characteristics of controlled polymerization.

Finally, we further investigated the influence of various reaction parameters on the polymerization behavior mediated by **4a**. Among the examined factors-including the monomer concentration, solvent, and temperature–temperature was found to have a pronounced impact on the isotactic selectivity of the catalyst (Table S2, entries 4–17). As shown in Fig. 2D, within the temperature range of 40 to 80 °C, P_m values increased with decreasing temperature. At 40 °C, a maximum P_m of 0.99 was achieved (Fig. S50), and the corresponding ^{13}C NMR spectrum displayed peak patterns closely resembling those of *L*-PEtG (Fig. 1A), confirming the high isotacticity of the polymer produced by **4a** under these conditions. This improvement in isotacticity was attributed to the reduced reactivity of the growing chain end at lower temperatures, which stabilized the chain conformations and thus favored isotactic propagation. Further lowering of the polymerization temperature did not result in a continued increase in isotacticity; instead, a slight decrease was observed. This was presumably due to the significantly reduced polymerization rate at lower temperatures, which prolonged the reaction time and slightly diminished the isotacticity.[57]

Thermal and mechanical properties

The correlation between the polymer sequence structure and material properties has long been a subject of considerable interest.[58] Given that the catalytic system developed in this study enabled the controlled synthesis of PEtG with varying sequence structures, the thermal, crystallization, and mechanical properties of the resulting polymers were systematically investigated (Tables S3 and S4). Differential Scanning Calorimetry (DSC) was first employed to determine the T_m of the polymers, as T_m provides a practical reference for polymer processing conditions. As shown in Fig. 4A and B, a progressive and orderly increase in T_m-from amorphous to 205 °C-was observed with increasing content of the highly crystalline [mmm] triad sequences. In particular, the highly *it*-PEtG synthesized using **4a** exhibited a T_m of 205 °C, representing a remarkable 97 °C enhancement compared to *L*-PEtG obtained *via* direct ROP of *L*-EtG. This substantial increase in T_m was likely due to the formation of isotactic stereoblock copolymer structures through the stereoselective ROP of *rac*-EtG catalyzed by **4a**, which promoted the development of stereocomplex crystallites with enhanced thermal stability. To validate this hypothesis, *L*-PEtG and *D*-PEtG were individually synthesized and subsequently blended in a 1 : 1 mass ratio to form stereocomplex PEtG (*sc*-PEtG), which was then compared with other PEtG samples in terms of thermal behavior. The DSC thermogram of *sc*-PEtG revealed a melting temperature of 208 °C, only 3 °C higher than that of the polymer obtained using **4a** (Fig. 4C), thereby confirming the stereoblock architecture and high stereoregularity of the **4a** produced PEtG.

Wide-angle X-ray diffraction (WAXD) patterns of different types of PEtG provided valuable insights into the polymer microstructures. As shown in Fig. 4D, *L*-PEtG exhibited crystalline diffraction peaks at $2\theta = 14.7°$, 17.2°, 23.2°, and 25.6°. *Sc*-PEtG displayed diffraction peaks at $2\theta = 10.7°$, 18.5° [19.3°(subpeak)], and 21.5°. Consistent with expectations, *it*-PEtG and *ir*-PEtG displayed diffraction peaks at positions identical to those of *sc*-PEtG, with no observable peaks corresponding to *L*-PEtG. Additionally, *ir*-PEtG exhibited significantly reduced peak intensities compared to *sc*-PEtG and *it*-PEtG, indicating a decrease in both crystalline regions and overall crystallinity. Notably, the formation of the stereocomplex structure substantially accelerated the crystallization rate of the polymer. Both low and high molecular weight *it*-PEtG crystallized at faster cooling rates, while *L*-PEtG did not show crystallization peaks at a cooling rate of 10 °C min^{-1} (Fig. S54).

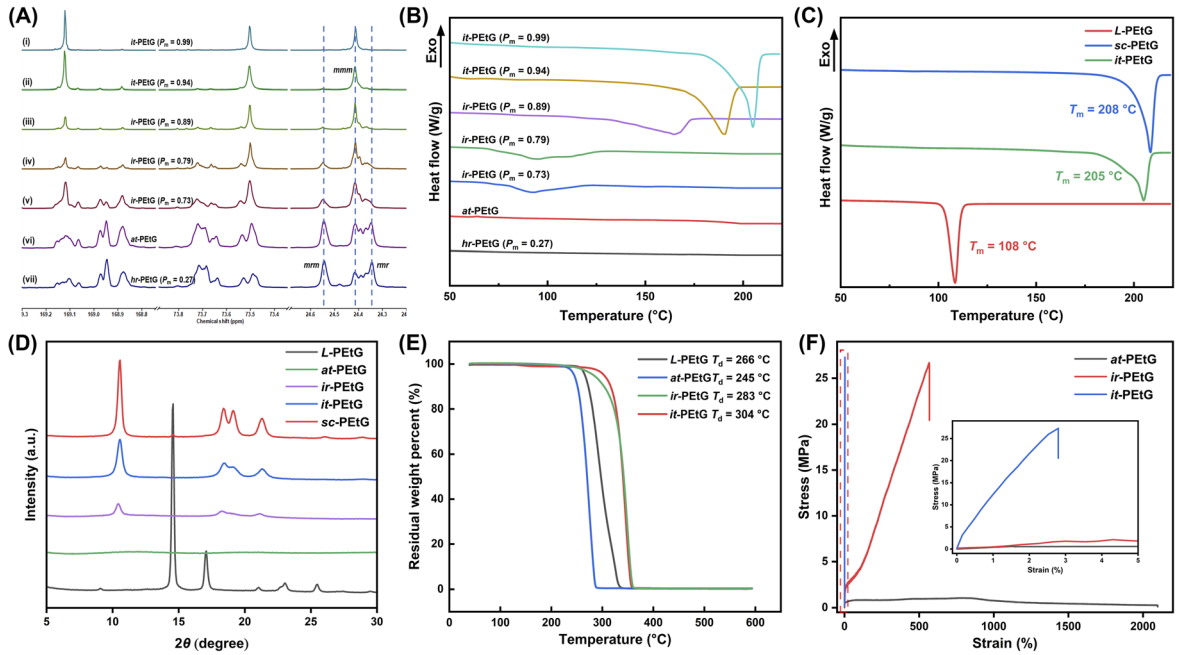

Fig. 4 Comparison of the performance of different types of PEtG. (A) Stacked quantitative ^{13}C NMR spectra of PEtG in $CDCl_3$ highlighting signals from the carbonyl, methine, and methylene regions. (B) DSC thermograms of *hr*-, *at*-, *ir*-, and *it*-PEtG. For Fig. A and B, the samples from top to bottom correspond to Table 1, entry 18; entry 4; entry 16; entry 8; entry 11; Table S2, entry 22 and Table 1, entry 12. (C) DSC thermograms of *L*-PEtG ($\Delta H_m = 35.6$ J g^{-1}, Table S2, entry 23), *sc*-PEtG ($\Delta H_m = 60.2$ J g^{-1}), and *it*-PEtG ($\Delta H_m = 51.6$ J g^{-1}, Table 1, entry 18) obtained using **4a** at 40 °C. (D) Powder XRD profile of *L*-, *at*-, *ir*-, *it*- and *sc*-PEtG. From bottom to top, the samples correspond to Table S2, entry 23; Table S2, entry 22; Table 1, entry 8; Table 1, entry 18 and the *L*-PEtG/*D*-PEtG (1 : 1 w/w) blend. (E) TGA of *L*-PEtG ($M_{n,GPC} = 94.3$ kDa, $Đ = 1.22$, Table S2, entry 25), *at*-PEtG ($M_{n,GPC} = 90.6$ kDa, $Đ = 1.25$, Table S2, entry 26), *ir*-PEtG ($P_m = 0.76$, $M_{n,GPC} = 100.2$ kDa, $Đ = 1.12$, Table 1, entry 20) and *it*-PEtG ($P_m = 0.94$, $M_{n,GPC} = 90.4$ kDa, $Đ = 1.08$, Table 1, entry 19). (F) Stress–strain curves of *it*-PEtG ($\sigma_b = 26.7 \pm 1.1$ MPa, $\varepsilon_b = 2.8 \pm 0.6\%$, $M_n = 90.4$ kDa, Table 1, entry 19), *ir*-PEtG ($\sigma_b = 26.7 \pm 0.9$ MPa, $\varepsilon_b = 569.9 \pm 36.5\%$, $M_n = 100.2$ kDa, Table 1, entry 20), and *at*-PEtG ($\sigma_b = 1.1 \pm 0.1$ MPa, $\varepsilon_b = 2119 \pm 220\%$, $M_n = 90.6$ kDa, Table S2, entry 26).

The thermal stability of high molecular weight PEtG exhibited a trend similar to that of the melting point, with the thermal decomposition temperature at 5% weight loss ($T_{d,5\%}$) gradually increasing as the [mmm] content increased. Notably, *it*-PEtG ($P_m = 0.94$) showed a $T_{d,5\%}$ of approximately 304 °C (Fig. 4E), which represented an increase of about 40 °C compared to that of *L*-PEtG. This enhancement was likely attributed to the higher crystallinity of *it*-PEtG relative to *L*-PEtG, resulting in improved thermal stability.

The relationship between the stereoregularity of PEtG and its mechanical properties was a central focus of this investigation. The resulting high molecular weight PEtG samples were processed into dumbbell-shaped specimens for tensile testing. As shown in Fig. 4F, *it*-PEtG exhibited strong yet brittle mechanical behavior (ultimate tensile strength $\sigma_b = 27.3 \pm 1.1$ MPa; elongation at break $\varepsilon_b = 2.8 \pm 0.7\%$) due to its highly regular polymer backbone and high crystallinity. In contrast, *at*-PEtG, with lower backbone regularity and reduced crystallinity, demonstrated high ductility ($\varepsilon_b = 2119 \pm 220\%$) but a low tensile strength ($\sigma_b = 1.1 \pm 0.1$ MPa). The *ir*-PEtG sample ($P_m = 0.77$), which exhibited an intermediate level of stereoregularity, showed a combination of high strength ($\sigma_b = 26.7 \pm 0.9$ MPa) and excellent toughness ($\varepsilon_b = 569.9 \pm 36.5\%$). Unfortunately, mechanical properties of *hr*-PEtG were not accurately determined due to its low molecular weight and viscous solid form. These findings clearly demonstrated that the stereomicrostructures of PEtG had a substantial impact on their mechanical properties and that the mechanical properties could be precisely tuned by controlling the microstructural regularity of the polymer.

The significant differences in toughness observed among PEtGs with different microstructures suggest that variations in crystallinity, induced by polymer stereoregularity may have a crucial impact on their mechanical performance (Fig. S57). This prompted us to conduct an in-depth investigation into how the crystallinity of PEtG-based materials influences their mechanical properties. Due to the poor crystallization ability of *L*-PEtG, we prepared *L*-PEtG* by incorporating a nucleating agent to enhance its crystallization behavior. The thermomechanical properties of *L*-PEtG, *L*-PEtG*, and *it*-PEtG were then compared under different crystallization conditions, including quenched and annealed crystallization (denoted as Q and C, respectively) (Tables S4 and S5). As shown in Fig. 5A and B, the quenched amorphous *L*-PEtG (*L*-PEtG-Q) exhibited the highest elongation at break, albeit with reduced yield strength. Upon annealing, *L*-PEtG-C displayed increased tensile strength but decreased elongation and toughness due to the growth of crystalline domains. Further enhancement in crystallinity in *L*-PEtG*-C led to the highest yield strength among all samples. As expected, the highly crystalline *it*-PEtG displayed brittle fracture

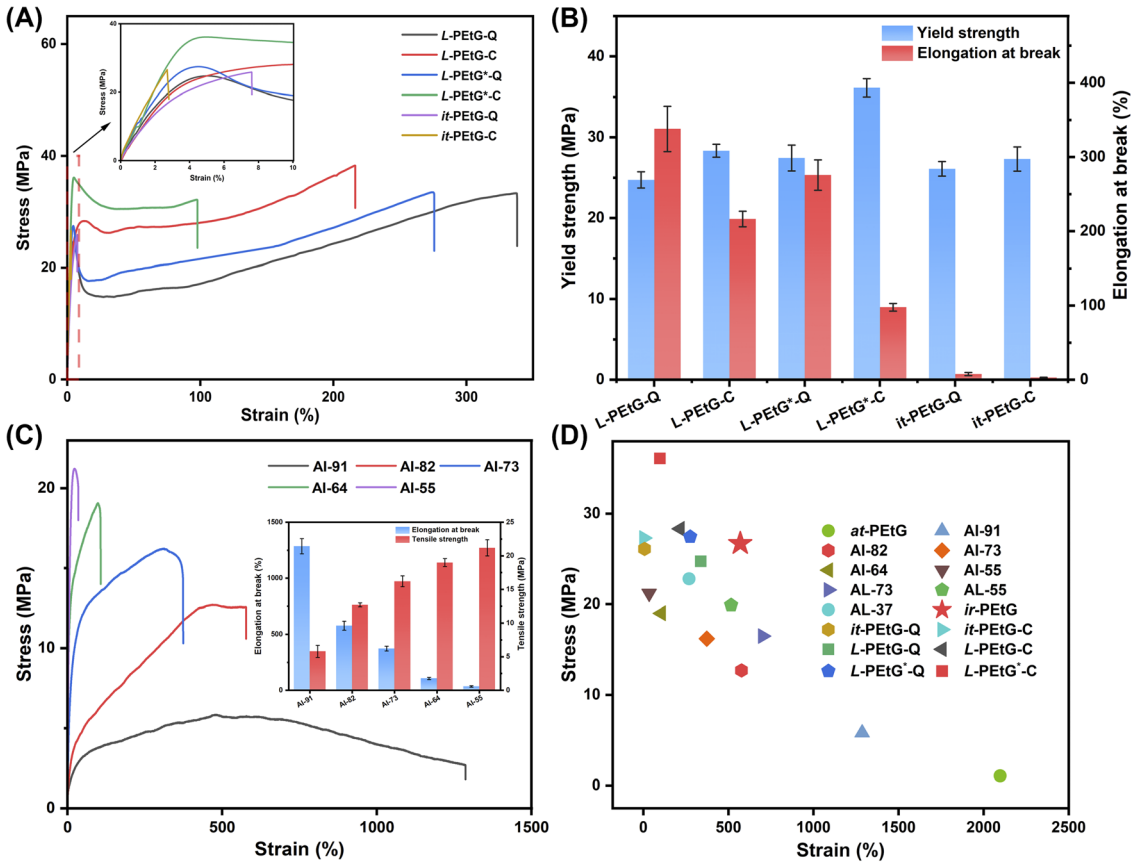

Fig. 5 (A) Stress–strain curves of *L*-PEtG, *L*-PEtG*, and *it*-PEtG after quenching and annealing crystallization treatment. (B) Comparison of mechanical properties of *L*-PEtG, *L*-PEtG*, and *it*-PEtG after quenching and annealing crystallization treatment. (C) Stress–strain curves of *at*-PEtG/*it*-PEtG blends (inserted picture: mechanical property comparison). (D) Overall mechanical property comparison of PEtG-based polymers.

behavior (Fig. S55). These results confirm that a proper balance between crystalline and amorphous domains within PEtG can enable simultaneous tuning of material hardness and toughness.

The improvement in toughness resulting from reduced stereoregularity was often challenged by property trade-off in the form of a decreased T_m. Encouraged by the above results, we explored a simple blending strategy using *at*-PEtG to toughen the brittle *it*-PEtG without compromising its superior thermo-mechanical properties. This approach also adheres to the principle of single-material product design. As shown in Fig. 5C, with increasing content of highly crystalline *it*-PEtG in the *at*-PEtG matrix, the tensile strength of the blends gradually increased, while the elongation at break and toughness decreased. This trend demonstrates that the mechanical properties of the blends can be finely tuned over a wide range by adjusting the blending ratio. Notably, owing to the high crystallizability of *it*-PEtG, all resulting blends exhibited high melting points (T_m = 176–182 °C) and rapid crystallization rates (Table S6). Similar trends in mechanical behavior were observed for blends of *L*-PEtG and *at*-PEtG (Fig. S56); however, these systems showed relatively poor crystallinity (Table S7). Overall, these findings highlight that by precisely tuning the microstructure and crystallinity of PEtG, it is possible to develop a new class of polyester materials with high melting points, excellent thermal stability, and broadly tunable mechanical performance (Fig. 5D and S57).

Conclusions

By rational catalyst design, we achieved the stereoselective ROP of *rac*-EtG, leading to PEtG-based polymers with high stereoregularity and tunable mechanical properties. Our results demonstrate that chiral catalysts governed by cooperative ESC and CEC mechanisms can produce polyesters with moderate isotacticity (P_m = 0.90). In contrast, achiral catalysts primarily governed by the CEC mechanism can yield highly isotactic polymers (P_m up to 0.99 and T_m = 205 °C) through judicious modification of substituents and polymerization conditions. The catalyst structure plays a pivotal role in influencing both polymerization activity and stereoselectivity. In particular, tuning the steric hindrance at the 3-position of the salicylaldehyde framework enables selective modulation of the polymer microstructure from atactic to isotactic to heterotactic configurations. Moreover, these catalysts exhibit excellent control over the polymerization process, allowing for the synthesis of high molecular weight polymers for detailed performance evaluation. An increase in [mmm] triad content

correlates with enhanced melting points and thermal stability. A balanced crystalline-amorphous domain in PEtG allows for simultaneous tuning of both strength and toughness, resulting in PEtG-based polyesters with widely adjustable mechanical performance. In summary, this efficient catalytic strategy affords bio-based polymers that not only reduce dependence on petroleum-derived resources but also introduce a generalizable approach to sequence-programmable polymer design through steric-hindrance-guided stereocontrol, offering a new paradigm for sustainable, high-performance plastic materials.

Author contributions

J. H.: conceptualization, data curation, methodology, writing – original draft, writing – review & editing, formal analysis; X. L.: data curation, formal analysis; W. W.: investigation; Y. D.: software; H. Z.: methodology, project administration; C. W.: funding acquisition, supervision; R. D.: validation, writing – review & editing; X. B.: supervision, validation, visualization; X. C.: supervision, resources.

Conflicts of interest

There are no conflicts to declare.

Data availability

The data supporting this article have been included as part of the SI.

Supplementary information includes detailed experimental procedures, materials, and methods; additional polymerization and characterization data (NMR, GPC, DSC and Stress-strain curves). See DOI: **https://doi.org/10.1039/d5sc05510e**.

Acknowledgements

This work was supported by the National Key Research and Development Program of China (No. 2021YFB3801901) and Tianjin Science and Technology Plan Project (No. 23YFYSHZ00060).

Notes and references

1 Y. Zhu, C. Romain and C. K. Williams, Sustainable polymers from renewable resources, *Nature*, 2016, **540**, 354–362.
2 C. Shi, E. C. Quinn, W. T. Diment and E. Y. X. Chen, Recyclable and (Bio)degradable Polyesters in a Circular Plastics Economy, *Chem. Rev.*, 2024, **124**, 4393–4478.
3 B. A. Abel, R. L. Snyder and G. W. Coates, Chemically recyclable thermoplastics from reversible-deactivation polymerization of cyclic acetals, *Science*, 2021, **373**, 783–789.
4 Y. Wang, R.-J. van Putten, A. Tietema, J. R. Parsons and G.-J. M. Gruter, Polyester biodegradability: importance and potential for optimisation, *Green Chem.*, 2024, **26**, 3698–3716.
5 S. Farah, D. G. Anderson and R. Langer, Physical and mechanical properties of PLA, and their functions in widespread applications — A comprehensive review, *Adv. Drug Delivery Rev.*, 2016, **107**, 367–392.
6 A. Z. Naser, I. Deiab and B. M. Darras, Poly(lactic acid) (PLA) and polyhydroxyalkanoates (PHAs), green alternatives to petroleum-based plastics: a review, *RSC Adv.*, 2021, **11**, 17151–17196.
7 R. M. Rasal, A. V. Janorkar and D. E. Hirt, Poly(lactic acid) modifications, *Prog. Polym. Sci.*, 2010, **35**, 338–356.
8 A. S. Narmon, A. Dewaele, K. Bruyninckx, B. F. Sels, P. Van Puyvelde and M. Dusselier, Boosting PLA melt strength by controlling the chirality of co-monomer incorporation, *Chem. Sci.*, 2021, **12**, 5672–5681.
9 H. Marubayashi and S. Nojima, Crystallization and Solid-State Structure of Poly(l-2-hydroxy-3-methylbutanoic acid), *Macromolecules*, 2016, **49**, 5538–5547.
10 M. Onur Arıcan and O. Mert, Symmetrical substituted glycolides: methodology and polymerization, *Polym. Chem.*, 2020, **11**, 4477–4491.
11 A. R. Craze, R. W. F. Kerr, T. M. McGuire, L. Wille and C. K. Williams, Toughened commercial poly(l-lactide) (PLLA) using degradable and recyclable poly(ester-alt-ether)-b-PLLA, *Green Chem.*, 2025, **27**, 9495–9511.
12 M. Yin and G. L. Baker, Preparation and Characterization of Substituted Polylactides, *Macromolecules*, 1999, **32**, 7711–7718.
13 T. Liu, T. L. Simmons, D. A. Bohnsack, M. E. Mackay, M. R. Smith and G. L. Baker, Synthesis of Polymandelide: A Degradable Polylactide Derivative with Polystyrene-like Properties, *Macromolecules*, 2007, **40**, 6040–6047.
14 S. Chen, Z. Jia, L. Cao, Y. Li, X. Han, X. Pan and J. Wu, AABB-Type Copolyester Synthesis via Highly Alternating Ring-Opening Copolymerization of Lactide and Benzylglycolide and Detailed Alternating Level Analyses, *Macromolecules*, 2021, **54**, 9027–9038.
15 Z. Jia, J. Jiang, X. Zhang, Y. Cui, Z. Chen, X. Pan and J. Wu, Isotactic-Alternating, Heterotactic-Alternating, and ABAA-Type Sequence-Controlled Copolyester Syntheses via Highly Stereoselective and Regioselective Ring-Opening Polymerization of Cyclic Diesters, *J. Am. Chem. Soc.*, 2021, **143**, 4421–4432.
16 J. Xian, H. Chen, G. Yao, F. Chen, Z. Chen, H. Cao, L. Cao, X. Pan, Y. Tang and J. Wu, Enantiomorphic Site-Assisted Chain End Control Stereospecific Alternating Copolymerization of Chiral Cyclic Diesters, *Angew. Chem., Int. Ed.*, 2024, **64**, e202420316.
17 X. Guo, G. Xu, R. Yang and Q. Wang, Specific Discrimination Polymerization for Highly Isotactic Polyesters Synthesis, *J. Am. Chem. Soc.*, 2024, **146**, 9084–9095.
18 G. Li, G. Xu, X. Guo, R. Yang, H. Sun and Q. Wang, Polymer Tacticity Control for Stereoselective Ring-Opening Polymerization of Racemic n-Propylglycolide, *ACS Catal.*, 2024, **14**, 1173–1182.
19 J. Hu, W. Wang, Y. Du, H. Zhang, Y. Liu, X. Bian, H. Sun and X. Chen, Efficient synthesis and performance investigation of poly(lactide) derivatives, *Acta Polym. Sin.*, 2025, **56**, 26–35.
20 H. Tsuji and A. Okumura, Stereocomplex Formation between Enantiomeric Substituted Poly(lactide)s: Blends of

Poly[(S)-2-hydroxybutyrate] and Poly[(R)-2-hydroxybutyrate], *Macromolecules*, 2009, **42**, 7263–7266.

21 A. Ghanbari and R. E. Prud'homme, Lamellar and spherulitic crystallization of poly(s-2-hydroxybutanoic acid) and its stereocomplexes, *Polymer*, 2017, **112**, 377–384.

22 K. Majerska and A. Duda, Stereocontrolled Polymerization of Racemic Lactide with Chiral Initiator: Combining Stereoelection and Chiral Ligand-Exchange Mechanism, *J. Am. Chem. Soc.*, 2004, **126**, 1026–1027.

23 G. Xu, Q. Mahmood, C. Lv, R. Yang, L. Zhou and Q. Wang, Asymmetric kinetic resolution polymerization, *Coord. Chem. Rev.*, 2020, **414**, 213–296.

24 M. J. L. Tschan, R. M. Gauvin and C. M. Thomas, Controlling polymer stereochemistry in ring-opening polymerization: a decade of advances shaping the future of biodegradable polyesters, *Chem. Soc. Rev.*, 2021, **50**, 13587–13608.

25 H. Li, R. M. Shakaroun, S. M. Guillaume and J. F. Carpentier, Recent Advances in Metal-Mediated Stereoselective Ring-Opening Polymerization of Functional Cyclic Esters towards Well-Defined Poly(hydroxy acid)s: From Stereoselectivity to Sequence-Control, *Chem.–Eur. J.*, 2019, **26**, 128–138.

26 Y. Zhong, Q. Feng, X. Wang, L. Yang, A. G. Korovich, L. A. Madsen and R. Tong, Photocatalyst-independent photoredox ring-opening polymerization of O-carboxyanhydrides: stereocontrol and mechanism, *Chem. Sci.*, 2021, **12**, 3702–3712.

27 M. J. Stanford and A. P. Dove, Stereocontrolled ring-opening polymerisation of lactide, *Chem. Soc. Rev.*, 2010, **39**, 486–494.

28 N. Spassky, M. Wisniewski, C. Pluta and A. Le Borgne, Highly stereoelective polymerization of rac-(D,L)-lactide with a chiral schiff's base/aluminium alkoxide initiator, *Macromol. Chem. Phys.*, 2003, **197**, 2627–2637.

29 J. W. Kramer, D. S. Treitler, E. W. Dunn, P. M. Castro, T. Roisnel, C. M. Thomas and G. W. Coates, Polymerization of Enantiopure Monomers Using Syndiospecific Catalysts: A New Approach To Sequence Control in Polymer Synthesis, *J. Am. Chem. Soc.*, 2009, **131**, 16042–16044.

30 Z. Zhou, A. M. LaPointe and G. W. Coates, Atactic, Isotactic, and Syndiotactic Methylated Polyhydroxybutyrates: An Unexpected Series of Isomorphic Polymers, *J. Am. Chem. Soc.*, 2023, **145**, 25983–25988.

31 Y. Lu and G. W. Coates, Pairing-Enhanced Regioselectivity: Synthesis of Alternating Poly(lactic-co-glycolic acid) from Racemic Methyl-Glycolide, *J. Am. Chem. Soc.*, 2023, **145**, 22425–22432.

32 M. S. Young, A. M. LaPointe, S. N. MacMillan and G. W. Coates, Highly Enantioselective Polymerization of β-Butyrolactone by a Bimetallic Magnesium Catalyst: An Interdependent Relationship Between Favored and Unfavored Enantiomers, *J. Am. Chem. Soc.*, 2024, **146**, 18032–18040.

33 Z. Zhong, P. J. Dijkstra and J. Feijen, [(salen)Al]-Mediated, Controlled and Stereoselective Ring-Opening Polymerization of Lactide in Solution and without Solvent: Synthesis of Highly Isotactic Polylactide Stereocopolymers from Racemic d,l-Lactide, *Angew. Chem., Int. Ed.*, 2002, **41**, 4510–4513.

34 Z. Zhong, P. J. Dijkstra and J. Feijen, Controlled and Stereoselective Polymerization of Lactide: Kinetics, Selectivity, and Microstructures, *J. Am. Chem. Soc.*, 2003, **125**, 11291–11298.

35 Z. Zhang, C. Shi, M. Scoti, X. Tang and E. Y. X. Chen, Alternating Isotactic Polyhydroxyalkanoates via Site- and Stereoselective Polymerization of Unsymmetrical Diolides, *J. Am. Chem. Soc.*, 2022, **144**, 20016–20024.

36 A. H. Westlie and E. Y. X. Chen, Catalyzed Chemical Synthesis of Unnatural Aromatic Polyhydroxyalkanoate and Aromatic–Aliphatic PHAs with Record-High Glass-Transition and Decomposition Temperatures, *Macromolecules*, 2020, **53**, 9906–9915.

37 X. Tang and E. Y. X. Chen, Chemical synthesis of perfectly isotactic and high melting bacterial poly(3-hydroxybutyrate) from bio-sourced racemic cyclic diolide, *Nat. Commun.*, 2018, **9**, 2345.

38 X. Tang, A. H. Westlie, L. Caporaso, L. Cavallo, L. Falivene and E. Y. X. Chen, Biodegradable Polyhydroxyalkanoates by Stereoselective Copolymerization of Racemic Diolides: Stereocontrol and Polyolefin-Like Properties, *Angew. Chem., Int. Ed.*, 2020, **59**, 7881–7890.

39 X. Tang, A. H. Westlie, E. M. Watson and E. Y. X. Chen, Stereosequenced crystalline polyhydroxyalkanoates from diastereomeric monomer mixtures, *Science*, 2019, **366**, 754–758.

40 A. Pilone, K. Press, I. Goldberg, M. Kol, M. Mazzeo and M. Lamberti, Gradient Isotactic Multiblock Polylactides from Aluminum Complexes of Chiral Salalen Ligands, *J. Am. Chem. Soc.*, 2014, **136**, 2940–2943.

41 K. Press, I. Goldberg and M. Kol, Mechanistic Insight into the Stereochemical Control of Lactide Polymerization by Salan–Aluminum Catalysts, *Angew. Chem., Int. Ed.*, 2015, **54**, 14858–14861.

42 R. Hador, A. Botta, V. Venditto, S. Lipstman, I. Goldberg and M. Kol, The Dual-Stereocontrol Mechanism: Heteroselective Polymerization of rac-Lactide and Syndioselective Polymerization of meso-Lactide by Chiral Aluminum Salan Catalysts, *Angew. Chem., Int. Ed.*, 2019, **58**, 14679–14685.

43 C. P. Radano, G. L. Baker and M. R. Smith, Stereoselective Polymerization of a Racemic Monomer with a Racemic Catalyst: Direct Preparation of the Polylactic Acid Stereocomplex from Racemic Lactide, *J. Am. Chem. Soc.*, 2000, **122**, 1552–1553.

44 P. Hormnirun, E. L. Marshall, V. C. Gibson, A. J. P. White and D. J. Williams, Remarkable Stereocontrol in the Polymerization of Racemic Lactide Using Aluminum Initiators Supported by Tetradentate Aminophenoxide Ligands, *J. Am. Chem. Soc.*, 2004, **126**, 2688–2689.

45 J. Bruckmoser, S. Pongratz, L. Stieglitz and B. Rieger, Highly Isoselective Ring-Opening Polymerization of rac-β-Butyrolactone: Access to Synthetic Poly(3-hydroxybutyrate) with Polyolefin-like Material Properties, *J. Am. Chem. Soc.*, 2023, **145**, 11494–11498.

46 M. D. Jones, L. Brady, P. McKeown, A. Buchard, P. M. Schäfer, L. H. Thomas, M. F. Mahon, T. J. Woodman and J. P. Lowe, Metal influence on the iso- and hetero-selectivity of complexes of bipyrrolidine derived salan ligands for the polymerisation of rac-lactide, *Chem. Sci.*, 2015, **6**, 5034–5039.

47 N. Nomura, R. Ishii, Y. Yamamoto and T. Kondo, Stereoselective Ring-Opening Polymerization of a Racemic Lactide by Using Achiral Salen– and Homosalen–Aluminum Complexes, *Chem.–Eur. J.*, 2007, **13**, 4433–4451.

48 P. Hormnirun, E. L. Marshall, V. C. Gibson, R. I. Pugh and A. J. P. White, Study of ligand substituent effects on the rate and stereoselectivity of lactide polymerization using aluminum salen-type initiators, *Proc. Natl. Acad. Sci. U.S.A.*, 2006, **103**, 15343–15348.

49 X. Pang, R. Duan, X. Li, C. Hu, X. Wang and X. Chen, Breaking the Paradox between Catalytic Activity and Stereoselectivity: rac-Lactide Polymerization by Trinuclear Salen–Al Complexes, *Macromolecules*, 2018, **51**, 906–913.

50 T. M. Ovitt and G. W. Coates, Stereochemistry of Lactide Polymerization with Chiral Catalysts: New Opportunities for Stereocontrol Using Polymer Exchange Mechanisms, *J. Am. Chem. Soc.*, 2002, **124**, 1316–1326.

51 Y. Lu, J. H. Swisher, T. Y. Meyer and G. W. Coates, Chirality-Directed Regioselectivity: An Approach for the Synthesis of Alternating Poly(Lactic-co-Glycolic Acid), *J. Am. Chem. Soc.*, 2021, **143**, 4119–4124.

52 R. E. Gawley, Do the Terms "% ee" and "% de" Make Sense as Expressions of Stereoisomer Composition or Stereoselectivity?, *J. Org. Chem.*, 2006, **71**, 2411–2416.

53 S. Liu, H. Li, N. Zhao and Z. Li, Stereoselective Ring-Opening Polymerization of rac-Lactide Using Organocatalytic Cyclic Trimeric Phosphazene Base, *ACS Macro Lett.*, 2018, **7**, 624–628.

54 S. Hörl, I. Chiorescu, J. Bruckmoser, J. Futter and B. Rieger, Influence of Ligand Design and Non-Covalent Interactions on the Isoselective Ring-Opening Polymerization of rac-ß-Butyrolactone using Salan and Salalen Rare-Earth Metal Catalysts, *Angew. Chem., Int. Ed.*, 2025, **64**, e202504513.

55 L. Falivene, Z. Cao, A. Petta, L. Serra, A. Poater, R. Oliva, V. Scarano and L. Cavallo, Towards the online computer-aided design of catalytic pockets, *Nat. Chem.*, 2019, **11**, 872–879.

56 M. Kamitani, K. Yujiri and H. Yuge, Hemisphere and Distance-Dependent Steric Analysis of PNN Iron Pincer Complexes Using SambVca 2.1 and Its Influence on Alkene Hydrosilylation, *Organometallics*, 2020, **39**, 3535–3539.

57 Y. Zhu, M. Li, Y. Wang, X. Wang and Y. Tao, Performance-Advantaged Stereoregular Recyclable Plastics Enabled by Aluminum-Catalytic Ring-Opening Polymerization of Dithiolactone, *Angew. Chem., Int. Ed.*, 2023, **62**, e202302898.

58 Z. Zhang, E. C. Quinn, J. K. Kenny, A. Grigoropoulos, J. S. DesVeaux, T. Chen, L. Zhou, T. Xu, G. T. Beckham and E. Y. X. Chen, Stereomicrostructure-regulated biodegradable adhesives, *Science*, 2025, **387**, 297–303.